AGU ADVANCING EARTH AND SPACE SCIENCES

AGU Advances

RESEARCH ARTICLE
10.1029/2025AV002053

Runoff Reconstructions and Future Projections Indicate Highly Variable Water Supply From Pacific Rim Water Towers

Weipeng Yue[1,2,3], Max C. A. Torbenson[2], Feng Chen[1,3,4,5], Frederick Reinig[2], Jan Esper[2,6], Edurne Martinez del Castillo[2], Shijie Wang[1,3], Xiaoen Zhao[1,3,4], Mao Hu[1,3,4], Yang Xu[1], Martín A. Hadad[7], Álvaro González-Reyes[8], Fidel A. Roig[7,8], Tiyuan Hou[1,3], Honghua Cao[1,3,4], Hechuan Wang[1], Heli Zhang[1,5], Junqiang Niu[1], and Youping Chen[1,3]

[1]Yunnan Key Laboratory of International Rivers and Transboundary Eco-Security, Institute of International Rivers and Eco-Security, Yunnan University, Kunming, China, [2]Department of Geography, Johannes Gutenberg University, Mainz, Germany, [3]State Key Laboratory for Vegetation Structure, Function and Construction (VegLab), Yunnan University, Kunming, China, [4]Southwest United Graduate School, Kunming, China, [5]Key Laboratory of Tree-ring Physical and Chemical Research of the China Meteorological Administration/Xinjiang Laboratory of Tree-ring Ecology, Institute of Desert Meteorology, China Meteorological Administration, Urumqi, China, [6]Global Change Research Institute (CzechGlobe), Czech Academy of Sciences, Brno, Czech Republic, [7]Laboratorio de Dendrocronología de Zonas Áridas-Instituto y Museo de Ciencias Naturales, Universidad Nacional de San Juan, CIGEOBIO (CONICET-UNSJ), San Juan, Argentina, [8]Instituto de Ciencias de la Tierra, Facultad de Ciencias, Universidad Austral de Chile, Valdivia, Chile

Peer Review The peer review history for this article is available as a PDF in the Supporting Information.

Key Points:

- A new dendrochronological network of 100 tree-ring sampling sites reconstructs Central China Water Tower (CCWT) runoff depth back to 1595 CE, revealing long-term hydrological variability
- Comparative analysis of Pacific Rim water towers shows the CCWT provides the most stable water supply, while the Tibetan Plateau is more prone to extreme runoff events
- Twenty-first century projections predict increased runoff across most Pacific Rim water towers, except the Northern Rocky Mountains, emphasizing the need for region-specific water management strategies

Supporting Information:

Supporting Information may be found in the online version of this article.

Correspondence to:

F. Chen and J. Esper,
feng653@163.com;
esper@uni-mainz.de

Citation:

Yue, W., Torbenson, M. C. A., Chen, F., Reinig, F., Esper, J., Martinez del Castillo, E., et al. (2026). Runoff reconstructions and future projections indicate highly variable water supply from Pacific Rim water towers. *AGU Advances*, *7*, e2025AV002053. https://doi.org/10.1029/2025AV002053

Received 22 AUG 2025
Accepted 31 OCT 2025

Author Contributions:

Conceptualization: Weipeng Yue, Feng Chen, Jan Esper
Data curation: Weipeng Yue, Shijie Wang

Abstract Anthropogenic climate change affects regional hydrological cycles and poses significant challenges to the sustainable supply of freshwater. The Central China water tower (CCWT) is the key source region feeding the Yangtze and Yellow Rivers, and its runoff is indispensable for the surrounding mega-city clusters. Here we present a reconstruction of CCWT runoff depth (RD) back to 1595 CE, based on a new dendrochronological network including 100 tree-ring sampling sites and an ensemble averaging approach that combines multiple regression models. Comparison of this reconstruction with similar records from six water tower regions along the Pacific Rim (Mongolian Plateau, Tibetan Plateau TP, Great Dividing Range, Southern and Northern Rocky Mountains, Andes Mountains) revealed that the CCWT provide the most stable water supply, while the TP to be most susceptible to extreme runoff events. Twenty-first century projections indicate generally increasing runoff across most Pacific Rim water towers, whereas the Northern Rocky Mountains are projected to decline substantially. We attribute the differences in runoff variability and projected trends across Pacific Rim water towers to their distinct geographies and synoptic climatic conditions. The long-term runoff reconstructions and projected changes highlighted in this study provide insights for adaptive management strategies in China and all other regions relying on supply from mountain water towers.

Plain Language Summary Human-caused climate change is creating major challenges for sustainable freshwater supply. The Central China Water Tower (CCWT), a key source for the Yangtze and Yellow Rivers, supports large populations and cities. In this study, we used tree-ring data from 100 sites to reconstruct CCWT runoff depth back to 1595 CE, offering a long-term view of water availability. We also compared CCWT runoff with records from six other Pacific Rim water towers, including the Mongolian Plateau, Tibetan Plateau (TP), Great Dividing Range, Northern and Southern Rocky Mountains, and Andes Mountains. The CCWT showed the most stable water supply over time, while the TP had more extreme fluctuations. Looking ahead, model projections suggest increasing runoff in most regions, but a decline in the Northern Rockies. These contrasting trends reflect differences in geography and climate patterns across regions. Our findings highlight the importance of understanding both past and future changes in mountain water resources and the need for region-specific water management strategies in a changing climate.

1. Introduction

The high mountains and subalpine regions of the Pacific Rim host the headwaters of many of the world's major rivers (Viviroli et al., 2011; Wohl, 2013) (Figure 1a). The extensive glaciers, lakes, wetlands, and dense tributary networks in this region are vital for maintaining regional biodiversity, the health of fluvial systems, water security, and the provision of ecosystem services including climate regulation (Viviroli & Weingartner, 2004;

Formal analysis: Weipeng Yue, Max C. A. Torbenson, Frederick Reinig, Edurne Martinez del Castillo
Funding acquisition: Weipeng Yue, Feng Chen
Investigation: Feng Chen, Shijie Wang, Xiaoen Zhao, Mao Hu, Yang Xu, Tiyuan Hou, Honghua Cao, Hechuan Wang, Heli Zhang, Junqiang Niu, Youping Chen
Methodology: Weipeng Yue, Shijie Wang, Martín A. Hadad, Álvaro González-Reyes, Fidel A. Roig
Project administration: Feng Chen
Resources: Feng Chen, Jan Esper
Supervision: Feng Chen, Jan Esper
Validation: Shijie Wang
Visualization: Weipeng Yue, Max C. A. Torbenson, Frederick Reinig, Jan Esper, Edurne Martinez del Castillo
Writing – original draft: Weipeng Yue
Writing – review & editing: Max C. A. Torbenson, Feng Chen, Frederick Reinig, Jan Esper, Edurne Martinez del Castillo, Shijie Wang, Xiaoen Zhao, Mao Hu, Martín A. Hadad, Álvaro González-Reyes, Fidel A. Roig

Vörösmarty et al., 2010; Zhu & Cai, 2023). However, under the dual pressures of global climate change and intensifying human activities (Esper et al., 2024; Hoegh-Guldberg et al., 2019; Karl & Trenberth, 2003), these high mountain and subalpine river source regions are facing growing challenges, including glacier retreat, lake shrinkage, wetland degradation, and altered runoff patterns (Sorg et al., 2012; Vuille et al., 2018). Understanding the characteristics of these hydrological changes and their driving mechanisms is crucial for projecting future water supply and demand and for developing adaptive management strategies to safeguard water security across the entire Pacific Rim region. Changes in runoff result from the interactions among various climatic and hydrological factors within the Earth system (Nguyen et al., 2020). Runoff depth is a key indicator of how precipitation is converted into runoff and is characterized by distinctive regional scale and cross-basin characteristics (Moore & Clarke, 1981). It represents the annual total volume of surface runoff generated per unit area, commonly expressed in millimeters (mm), and can be regarded as an areal equivalent of streamflow. Runoff depth reflects the surface runoff generation capacity and runoff intensity within the hydrological cycle and is directly influenced by climate change and human activities (L. Wu et al., 2020). Climate change alters the spatial and temporal distribution of precipitation, evapotranspiration, and snowmelt, thereby causing changes in hydrological conditions and leading to non-stationary behavior and variations in RD (Li et al., 2024; Y. Wu et al., 2022).

However, it remains unclear whether the observed trends in RD within water source regions reflect natural variability or significant changes beyond long-term natural variability. To improve future runoff predictions and to develop effective climate adaptation strategies, it is necessary to compare current runoff levels with historical data and to identify the climatic drivers of runoff changes (An et al., 2022; Nguyen et al., 2020; Viorica et al., 2023). Reliable proxy data from archives such as ice cores, lake sediments, the shells of marine organisms, and tree rings offer valuable insights into large-scale climate and hydrological changes prior to the instrumental observation era (PAGES Hydro2k Consortium, 2017; Smerdon et al., 2023; Smith et al., 2002; Torbenson & Stagge, 2021; Tozer et al., 2016; Williams et al., 2020; H. Yan et al., 2021). Over the past few decades, extensive research in the high mountain and subalpine regions of the Pacific Rim has leveraged high-resolution tree-ring data to reconstruct hydrological changes in various watersheds (Cao et al., 2025; F. Chen et al., 2019a, 2019b; Cleaveland, 2000; X. Gou et al., 2010; Hadad et al., 2021; Islam et al., 2024; Y. Liu et al., 2020; Ljungqvist et al., 2020; Martin et al., 2019; Meko et al., 2001, 2022; Rao et al., 2020; Woodhouse & Lukas, 2006; Y. Wu et al., 2022; Y. Zhao et al., 2023). Such efforts have made important contributions to both theoretical and applied hydrological research, while also advancing interdisciplinary studies. However, most of these studies have focused on individual watersheds, and we have a more limited understanding of large-scale, cross-basin spatial relationships.

The Central China water tower (CCWT, Figure 1b) is the sole high-altitude water source region supplying the middle and lower reaches of the Yangtze and Yellow Rivers, providing essential social, ecological, cultural, and economic services to numerous megacities with populations exceeding 10 million (F. Chen, Wang, Dong, et al., 2024; Y. Liu et al., 2020; Nguyen et al., 2020). Reported research findings indicate that the water balance within the CCWT exhibits a long-term drying trend that exceeds the historical context of past centuries (Fang et al., 2010; Gao et al., 2021; N. Liu et al., 2019; C. Sun & Liu, 2019). However, without exception, these findings are limited by proxy data collected on a relatively small spatial scale, and they cannot represent moisture signal changes on cross-basin scales. In this study, we first developed a dendrochronological network using a dense tree-ring data set to reconstruct changes in the RD of the CCWT. Then, using data from drought atlases, we reconstructed the RD for the major river source regions across the Pacific Rim, including the Mongolian Plateau (MG), Tibetan Plateau (TP), Great Dividing Range (GDR), Northern Rockies (NR), Southern Rockies (SR), and Central Andes (CA) (Figure 1a). Finally, we place the runoff dynamics of the CCWT and other Pacific Rim water towers within a common spatiotemporal framework to assess the potential of the long-term water supply capacity of these water towers in the context of global change. Our objectives are to examine the frequency, intensity, and joint occurrence probabilities of extreme hydrological events within these water towers; to identify trends and stationarity characteristics of hydrological changes under past and future scenarios.

2. Data and Methods

2.1. Proxies and Hydrological Data

Numerous tree-ring samples from the CCWT were integrated with the aim of establishing a spatially extensive tree-ring sample network. This network is based on five tree species: *Pinus tabuliformis*, *Pinus bungeana*, *Pinus*

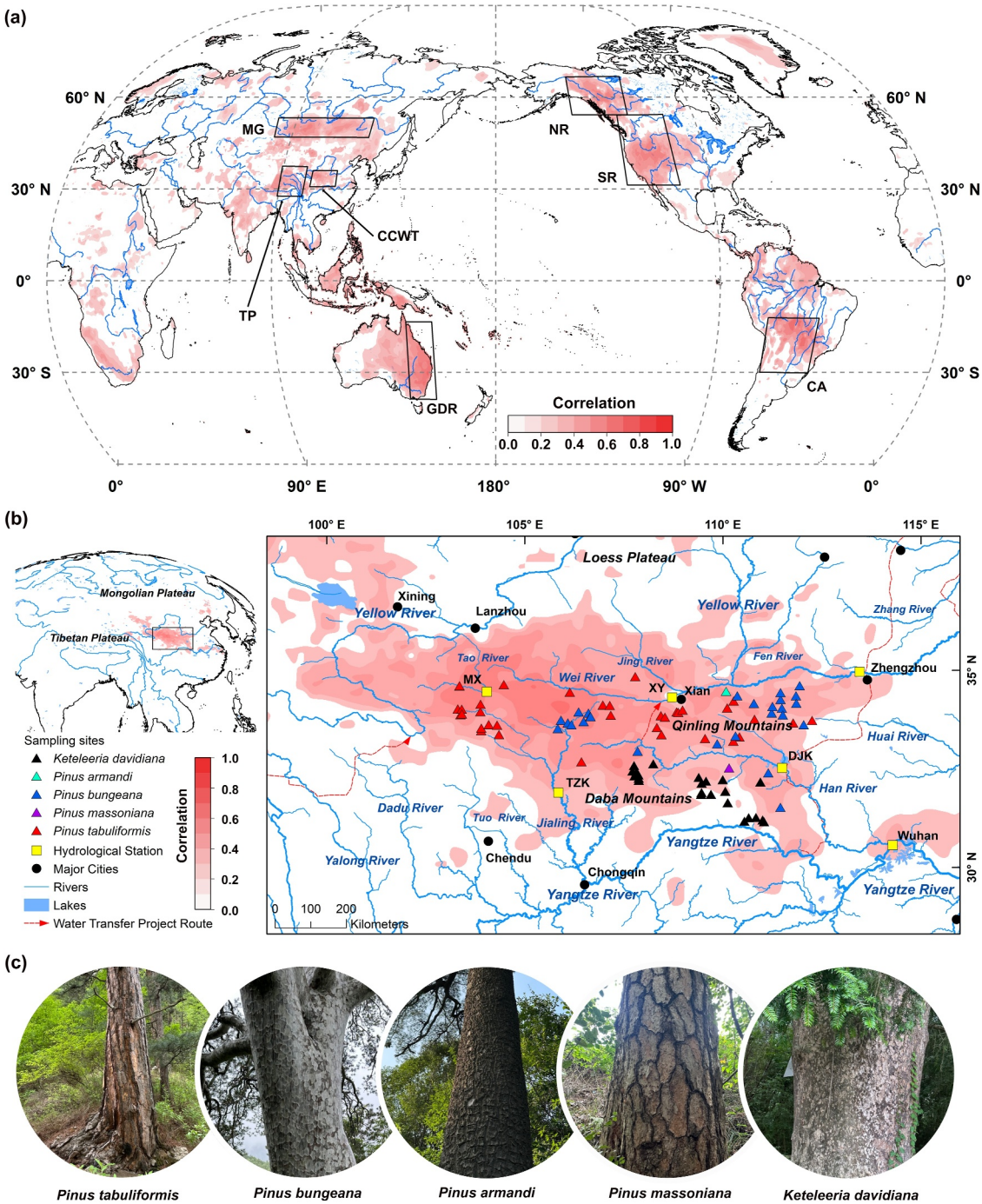

Figure 1. Spatial distribution of the Pacific Rim water towers and geographical characteristics of the Central China water tower (CCWT). (a) Spatial correlation analysis results between reconstructed and observed gridded runoff depths (G-RUN ENSEMBLE) in the Pacific Rim water towers during the validation period. The study areas include the CCWT, Mongolian Plateau, Tibetan Plateau, Great Dividing Range, Northern Rockies, Southern Rockies, and Central Andes. Darker red indicates a higher explained variance of the covariation, while areas that did not pass the 95% significance level are masked. (b) Spatial distribution of tree-ring sampling sites, hydrological stations, and fundamental geographical features. The color-mapped area represents the spatial correlation between the reconstructed runoff depth and gridded hydrological observations (CNRD v1.0). (c) Physical photos of the five sampled tree species, including *Pinus tabuliformis*, *Pinus bungeana*, *Pinus massoniana*, *Pinus armandi*, and *Keteleeria davidiana*.

massoniana, *Pinus armandi*, and *Keteleeria davidiana* (Figure 1, Figure S1 and Table S1 in Supporting Information S1). It encompasses over 1,110 individual trees and more than 2,000 separate cores, comprising a robust and regionally comprehensive dendrochronological data set (Figure 2a and Table S1 in Supporting Information S1).

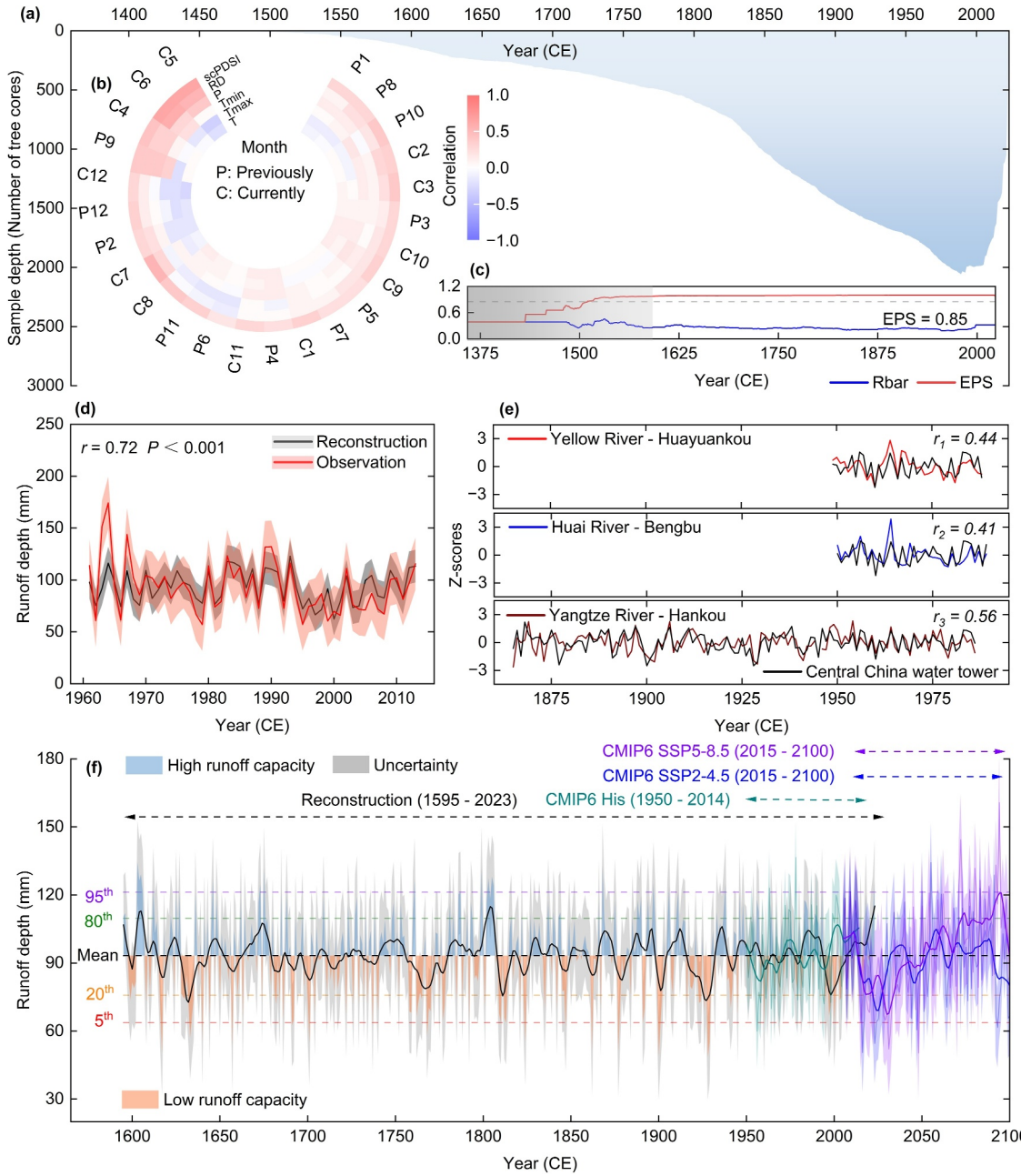

Figure 2. Process and results of runoff depth (RD) reconstruction and projection in the Central China water tower (CCWT) from January to June. (a) Variation in sample depth of regional tree-ring width chronology. (b) The correlation and hierarchical clustering analysis of regional tree-ring width chronology and meteorological and hydrological elements were presented using polar coordinate heat maps. The meteorological and hydrological elements were self-calibrated Palmer Drought Index (scPDSI), RD, total precipitation (P), mean minimum temperature (T_{min}), mean maximum temperature (T_{max}), and mean temperature (T). (c) The temporal variation characteristics of the Expressed Population Signal and Mean Inter-series Correlation (Rbar) of the regional tree-ring width chronology, with shaded areas indicating the truncated periods that do not meet the reconstruction standards. (d) Comparison between the multi-model ensemble mean reconstruction and observed RD for the CCWT during the instrumental period (1961–2013), with the shaded area representing the uncertainty range of ±1 standard deviation. (e) The CCWT relationship with the water supply to three major rivers, including the Yellow River, Huai River and Yangtze River (Figure S6 in Supporting Information S1, hydrological data come from the Global Runoff Data Center). (f) Reconstructed and projected RD in the CCWT. An 11-year window with the LOWESS method is applied for low-pass filtering to capture the decadal variability in reconstructed RD (black line).

The width measurement series were aggregated into a regional sample and processed using RCSsigFree (E. R. Cook & Kairiukstis, 2013; Homfeld et al., 2024; Speer, 2010). This program applies the Friedman variable-span smoothing function to remove growth trends and standardize the ring-width sequences (Maxwell et al., 2017; Yue,

Chen, Davi, et al., 2024). After 15 iterative steps in the RCS signal-free process, the error convergence stabilized, producing two key chronologies: the standard chronology and the signal-free chronology (McPartland et al., 2020) (Figure S2 in Supporting Information S1). To minimize the influence of local effects and ensure that the chronology better captures large-scale climate signals, we selected the more robust StdStb (Standard Chronology Stability) as the final reconstruction chronology (Deng et al., 2014). Additionally, we applied a stringent truncation criterion for defining the reliable reconstruction period: the starting year required coverage from at least three sampling directions within the study area; this aimed to reduce the artifact of "false signals" caused by overrepresentation from individual sampling sites (H. Wu et al., 2024). As a result, the reliable reconstruction period was truncated to begin in 1595, covering the years from 1595 to 2023 CE (Figure 2c, Figure S2 and Table S1 in Supporting Information S1).

In regions where dense tree-ring networks were unavailable, we utilized paleoclimatic drought atlases as proxy data sets (E. R. Cook, Anchukaitis, et al., 2010; E. R. Cook, Seager, et al., 2010; Morales et al., 2020; Palmer et al., 2015) (Figure S3 and Table S2 in Supporting Information S1). Tree-ring-based drought atlases are effective paleoclimate indicators for runoff reconstructions, supported by extensive prior research, which provide a solid foundation in terms of physical basis, theoretical framework, and applied practices (Nguyen et al., 2020). To address the challenge of insufficient fine-scale alignment between gridded hydrological data and observed measurements in the East Asian region, we collected hydrological data from stations in key basins (hydrological stations: MX, XY, TZK, DJK) (Figure 1 and Table S3 in Supporting Information S1). By summing the monthly mean streamflow data (m^3/s) from hydrological stations and converting it to total runoff volume, we calculated the corresponding RD (mm) by dividing by the combined drainage area of these basins (~217,224 km^2). This area accounts for approximately 69% of the CCWT and provides a representative benchmark for validating the reconstructed RD. For the TP, we utilized the China Natural Runoff Data set (CNRD v1.0), which has been validated as being superior to global runoff data sets in capturing the spatial distribution of water resources under the region's complex terrain and climate variability (J. Gou et al., 2021; Miao et al., 2022, 2024; Zhang et al., 2022) (Table S3 in Supporting Information S1). For other water towers, we adopted the Global RUNoff ENSEMBLE (G-RUN) data set (Ghiggi et al., 2019). This product leverages machine learning algorithms to estimate global runoff rates from observational data (Global Streamflow Indices and Metadata Archive, Do et al., 2018), thereby reducing reliance on the complex physical parameterizations of traditional hydrological models and enhancing both accuracy and robustness (Ghiggi, Humphrey, Seneviratne, & Gudmundsson, 2021; Yi et al., 2023) (Table S3 in Supporting Information S1). Although these data sets differ in origin and methodology, our comparisons target trends and variability rather than absolute values, minimizing dataset-specific biases and enabling meaningful assessments of runoff dynamics across water tower regions.

2.2. Historical Runoff Depth Reconstruction

We used an ensemble averaging approach combining multiple regression models to reconstruct RD across various water towers (Porporato & Ridolfi, 1997; Yue, Chen, Torbenson, et al., 2024; X. Zhao et al., 2023). This ensemble includes five linear regression models (Linear Regression, Ridge Regression, Lasso Regression, ElasticNet Regression, Huber Regression), and three machine learning models (Random Forest, Gradient Boosting, Extreme Gradient Boosting) (Biau & Scornet, 2016; T. Chen, 2015; Hans, 2011; Marquardt & Snee, 1975; McDonald, 2009; Montgomery et al., 2021; Natekin & Knoll, 2013; Ranstam & Cook, 2018; Rigatti, 2017; Su et al., 2012; Q. Sun et al., 2020; Zou & Hastie, 2005) (Tables S4 and S5 in Supporting Information S1). Prior to the reconstruction work, we used proxy data and hydrological data for correlation analysis to determine the best reconstructed hydrological season (E. R. Cook et al., 2013). The correlation analysis was focused on the period after 1950, when the observational quality of hydrological records improves and aligns with the coverage of the proxy data (Yue et al., 2023; Yue, Chen, Davi, et al., 2024). Seasonal correlation analysis identified the optimal reconstruction window for RD in each water tower, corresponding to the months with the highest explained variance: January–June (CCWT, 48.4%), July–August (Mongolian Plateau, 51.9%), January–August (TP, 50.4%), previous September–current April (GDR, 75.8%), June–August (NR, 56.9%), February–December (SR, 49.9%), and November–January (CA, 42.0%). Due to the seasonal lag effect of proxy data in capturing hydrological signals, it is difficult to coordinate nearly perfect unified hydrological seasons (Ziaco et al., 2020), but these monthly combinations represent the major activity in the hydrological system: that is most of them record the changes in RD during the flood season (Figure 2b and Figure S4 in Supporting Information S1). The training set and test set of the samples were randomly allocated in a ratio of 7:3 (Batista et al., 2004). The leave-one-out cross-

validation method and eight standard hydrological statistics were used to evaluate the performance of the reconstructed models, including: variance explanation (R^2), relative error percentage (RE1), product mean multiplication (PMT), error reduction value (RE2), sign test, Nash-Sutcliffe model efficiency coefficient (NSEC), root mean square deviation, and Klingupta efficiency (KGE) (Yue, Chen, Torbenson, et al., 2024) (Tables S6–S12 in Supporting Information S1). The regression results show that the average of the multi-model ensemble is superior to a single linear regression model in various statistical indicators, while reducing the overfitting defect of the machine learning method. The recording accuracy of the hydrological data measured by the instruments in earlier years may decline, so grid and proxy hydrological data outside the reconstruction area are also used to verify the stability and reliability of the reconstruction results (Figure S6 in Supporting Information S1).

2.3. Future Runoff Depth Projections

The total runoff parameters from 24 CMIP6 models were ensemble-averaged to evaluate the future hydrological changes in the Pacific Rim water towers (Eyring et al., 2016) (Table S13 in Supporting Information S1). Bias correction, bilinear interpolation, and variance scaling were applied to produce high-resolution and statistically adjusted runoff projections from CMIP6 ensemble outputs (Xu et al., 2021). First, the G-RUN data set was selected as the observational reference (Ghiggi et al., 2019). While station observations provide greater local accuracy, their fragmented coverage and temporal inconsistencies limit their use in cross-regional comparisons (Gudmundsson et al., 2018). G-RUN offers a spatially complet. alternative, enabling a uniform correction framework across all study areas (Ghiggi et al., 2019). We compared GRUN with in situ observations across multiple regions, and overall, GRUN's performance was satisfactory (Figures S7 and S8 in Supporting Information S1). Bilinear interpolation was applied to resample both the G-RUN and the CMIP6 ensemble data sets to a uniform spatial resolution of $0.5° \times 0.5°$. Subsequently, the ensemble empirical mode decomposition was used to separate the long-term nonlinear trends and perturbation components in both G-RUN and CMIP6 (Z. Wu & Huang, 2009). The perturbation components of CMIP6 were then scaled by a factor, which is the ratio of the standard deviations of the G-RUN and CMIP6 perturbation components. The scaled perturbation components were added to the G-RUN long-term nonlinear trend to produce the bias-corrected CMIP6 results for the historical period (1950–2014). For the future projection period (2015–2100), the same bias correction process was followed. Despite the adjustments in scale and bias, interannual variability in the projections remains prone to over- or underestimation. To address this, further scaling was performed to ensure consistency in both the mean and standard deviation, enabling a robust comparison of RD between CMIP6 projections, reconstructions, and observations during the overlapping period (F. Chen, Wang, Dong, et al., 2024; F. Chen, Wang, Zhao, et al., 2024; Y. Zhao et al., 2023; Yue, et al., 2025) (Figure 2 and Figure S9 in Supporting Information S1).

2.4. Analysis of Variability Characteristics

Based on the smoothed results (Locally Weighted Scatterplot Smoothing, LOWESS), periods when the RD remains above or below the mean for over 10 years are identified as periods of high runoff capacity (strong performance) or low runoff capacity (weak performance), respectively (Cleveland & Devlin, 1988). The 95th and 5th percentiles define threshold values for extreme flood and drought events, while the 80th and 20th percentiles are used as thresholds for the occurrence of flood and drought events (Morales et al., 2023) (Figure 2). In the kernel density estimation, the continuous probability density curve is generated by applying the Kernel smoothing method and then using the Scott bandwidth to balance the estimation bias and variance (Wand & Jones, 1994). For the distribution characteristics of extreme hydrological events, we used non-parametric Gaussian kernel function analysis to estimate the event rate based on the identified extreme event years. These rates, referenced against the full reconstruction period, were then used to calculate the return periods of such events (Morales et al., 2020, 2023). At the same time, 40-year bandwidth kernel smoothing is used to determine continuous long-term probability changes. The event list is resampled in 1,000 bootstrap simulations to add a 95% horizontal confidence interval (CI) to increase the credibility of the probability estimate (Hadad et al., 2021; Muñoz et al., 2016) (Figure 3).

For the analysis of hydrological drought and pluvials periods, we focused on understanding the duration and severity of Pacific Rim water tower runoff depths below or above the long-term mean, as well as their joint occurrence probabilities (Hessl et al., 2018). First, we applied run theory to classify the reconstructed runoff depths based on their duration and average severity, conditioned on runoff being lower or higher than the mean value over the entire period (X. Wang et al., 2017; R. Wu et al., 2019). Subsequently, we used Copula functions to

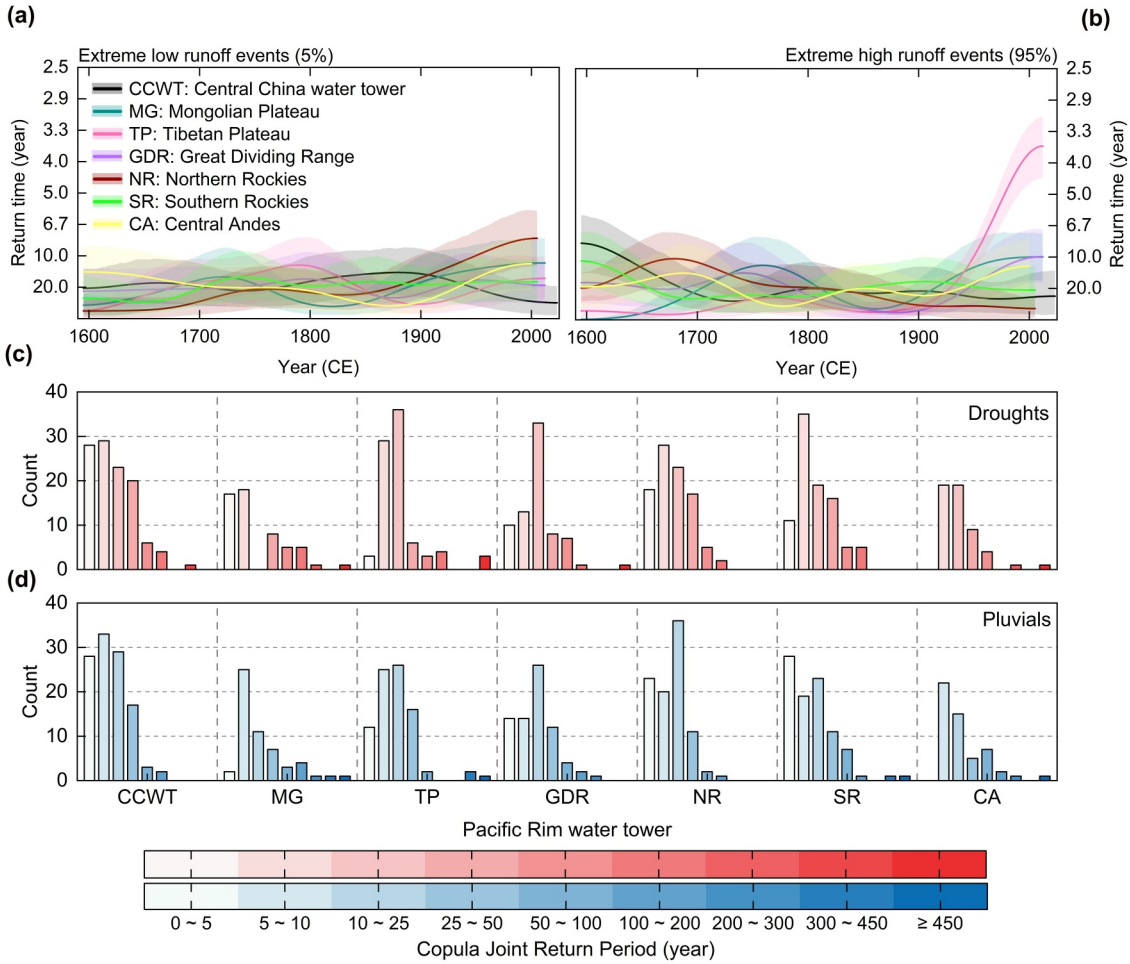

Figure 3. Estimating return intervals of extreme hydrological events and joint return periods of droughts and pluvials from reconstructed runoff depth in the Pacific Rim water towers. Extreme hydrological events are identified based on the 5th (a) and 95th (b) percentile thresholds, the bandwidth represents a 95% confidence interval, created from 1,000 bootstrapped resamples of the annual event list. The counts of joint return periods for droughts (c) and pluvials (d), based on the joint probabilities of mean severity and duration estimated by the Copula function, with the specific return period distributions shown in Figure S12 in Supporting Information S1. Darker bar colors indicate higher joint return periods.

estimate the joint probabilities of drought and flood durations and severities in the reconstructed runoff depths, ultimately deriving estimates of return periods (Hessl et al., 2018). Copula functions, which connect two or more marginal distributions into a multivariate distribution, were utilized due to their ability to automatically select the best-fitting copula model, based on the marginal distribution characteristics of each random variable. This approach avoids the need for specifying a more complex joint distribution (S. X. Chen & Huang, 2007; Sklar, 1973; J. Yan, 2007) (Figure S12 in Supporting Information S1).

To evaluate the stationarity characteristics of reconstructed runoff depths in the Pacific Rim water towers, we employed moving average smoothing to highlight long-term trends in the time series (Y. Wu et al., 2020). The selection of an optimum moving window is debated, but there is a consensus that longer windows are preferable (Mudelsee, 2014). Based on numerous successful applications, we selected a 40-year moving window (Y. Wu et al., 2020). This aligns with the length of the validation period, minimizes overfitting to shorter trends, and enhances the sample richness for confidence level estimation. The process involved calculating the 40-year backward-moving averages for all reconstructed time series and then performing two-sided *t*-tests to determine whether the mean state changes between the observed data and reconstructed runoff depths were statistically significant within each moving window (Y. Wu et al., 2022). Additionally, block bootstrap methods were employed to randomly resample the observed runoff data set to estimate the 95% confidence intervals for mean states, while preserving the statistical characteristics of the observed data (Noguchi et al., 2011; Razavi

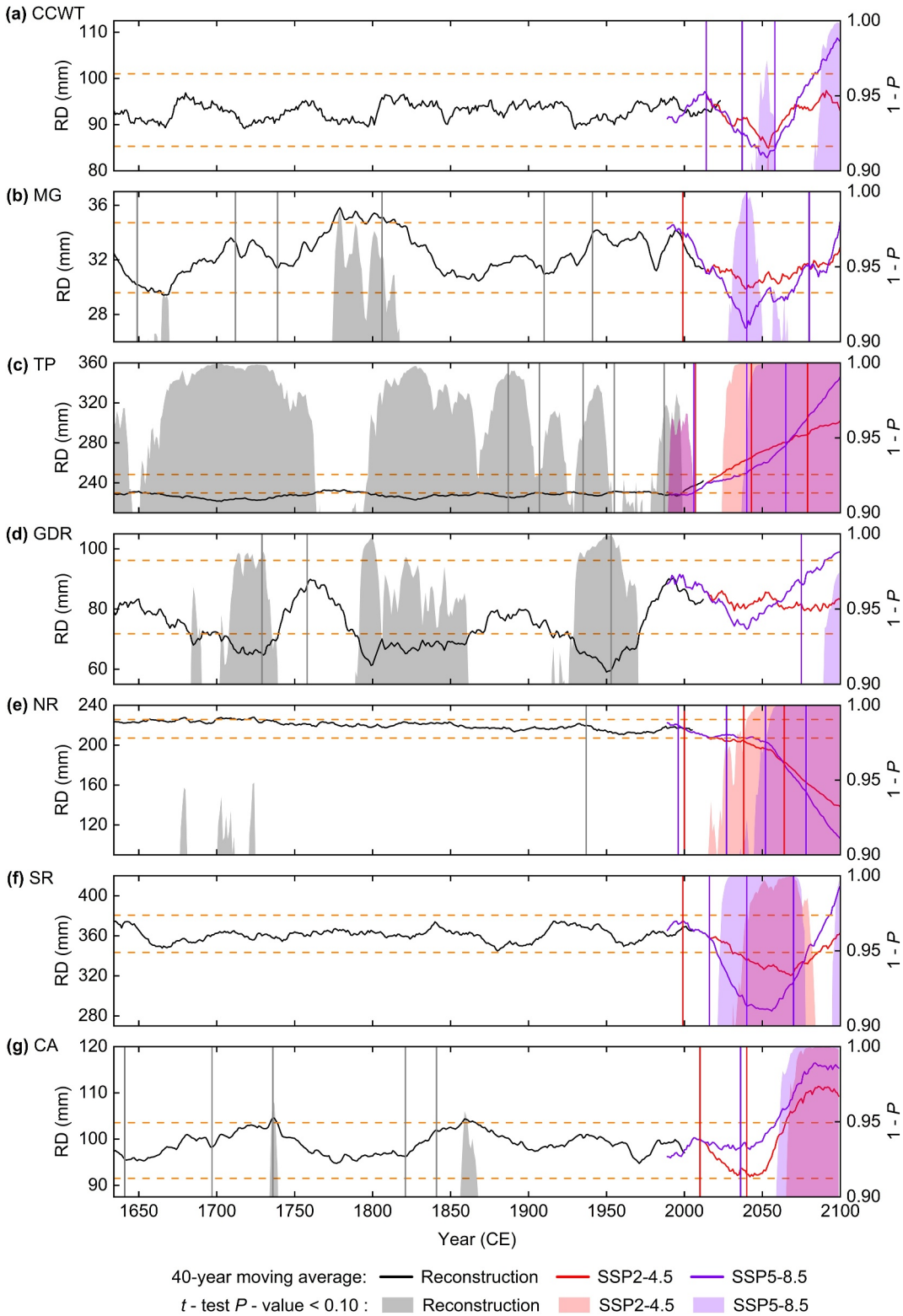

Figure 4.

et al., 2015) (Figure 4). For the detection of critical points in trend state changes, we chose the E-divisive method, which identifies change points based on statistical distance (Matteson & James, 2014). It employs a permutation test to assess the significance of change points, does not assume any specific data distribution, and is widely used in time series analysis (Y. Wu et al., 2020).

3. Results and Discussion

3.1. Reconstruction and Future Projection of Runoff Depth in the Central China Water Tower

Correlation analysis between the CCWT tree-ring network chronology (Figure 1 and Figure S2 in Supporting Information S1) and meteorological-hydrological data indicates a strong sensitivity to moisture conditions during April to June of the current year and September of the previous year, including RD, scPDSI, and precipitation (Figure 2b and Figure S4 in Supporting Information S1). Seasonal correlation analysis with RD further shows that the January–June period explains the highest proportion of variance (Figure S4 in Supporting Information S1). Although this season does not encompass an entire hydrological year, it includes multi-seasonal hydrological characteristics ranging from the winter low-flow period to the summer flood season (Figure S4 in Supporting Information S1). The reconstruction results indicate that the longest periods of strong surface runoff generation capacity in the CCWT were during 1663–1679 CE and 1827–1843 CE, and the longest period of weak surface runoff generation capacity was during 1756–1779 CE (Figure 2f). A total of 86 hydrological drought events occurred below the 20th percentile, including 23 extreme hydrological drought events below the 5th percentile. Overall, hydrological drought events accounted for 20% of the entire reconstruction period. Similarly, 86 hydrological flood events were observed above the 80th percentile, including 22 extreme hydrological flood events above the 95th percentile. The lowest RD during the entire reconstruction period was in 1928, at 47.95 mm, coinciding with the onset of the severe drought in the Shaanxi-Gansu region, which lasted for 18 consecutive months and led to a devastating famine (F. Chen, Wang, Dong, et al., 2024; F. Chen, Wang, Zhao, et al., 2024). The highest RD occurred in 1603 CE, exceeding the extreme flood event threshold by 13.4 mm, when historical records indicate widespread flooding across the Yellow-Huai-Hai River Basin (Yue, Chen, Torbenson, et al., 2024). Comparison of the reconstruction and observational records also confirms that the Yellow River, Huai River, and Yangtze River basins maintain a close hydrological relationship. Specifically, the reconstructed RD of the CCWT shows a significant positive correlation with the observed runoff at hydrological control stations in the middle and lower reaches of these basins ($r_1 = 0.44$, $r_2 = 0.41$, $r_3 = 0.56$; $p < 0.01$) (Figure 2e and Figure S6 in Supporting Information S1). This indicates that the interannual and interdecadal changes in RD in the CCWT profoundly impact hydrological variations in the surrounding basins. It also suggests that runoff changes in the three major basins of the eastern monsoon region exhibit a consistent response to extreme events (F. Chen, Wang, Dong, et al., 2024; Nguyen et al., 2020).

The downscaling and bias-correction projections of CMIP6 climate model ensembles provide a longer-term perspective on the future runoff generation capacity of the CCWT (Figure 2f) (Table S13 in Supporting Information S1). From the smoothed decadal trend, the CCWT's runoff generation capacity showed a fluctuating upward trajectory during the historical period (1950–2014). However, since 2011, a sustained decline has been projected, reaching a minimum in the 2030s under both the medium-emission (SSP2-4.5) and high-emission (SSP5-8.5) scenarios. Following this decline, the trend begins to reverse, with a fluctuating recovery lasting until the 2080s, after which there is a further steep decline toward the end of the century. Notably, the upward trend under SSP5-8.5, especially from the 2060s onwards, surpasses that of SSP2-4.5, indicating that RD would increase more linearly in line with rapid fossil fuel-driven economic growth compared to the moderate sustainable development pathway. Based on the hydrological event classification thresholds derived from the reconstructed RD, CCWT exhibits more drought events than flood events under the SSP2-4.5 scenario, while the number of extreme drought and extreme flood events remains equal (Table S14 in Supporting Information S1). In contrast,

Figure 4. Stability analysis of reconstructed and projected runoff depth (RD) series for the Pacific Rim water towers. (a) Central China Water Tower, (b) Mongolian Plateau, (c) Tibetan Plateau, (d) Great Dividing Range, (e) Northern Rockies, (f) Southern Rockies, and (g) Central Andes. All series use a 40-year backward moving average to highlight the long-term trends. The black, red, and purple lines represent the moving average results for the reconstructed series, and SSP2-4.5 and SSP5-8.5 scenarios, respectively. The gray, red, and purple shaded bars indicate periods where reconstructed, SSP2-4.5 projected, and SSP5-8.5 projected runoff depths differ significantly ($p < 0.10$) from observed runoff depths, based on two-sided *t*-tests. The orange dashed line represents the 95% confidence interval of the mean observed RD. The gray, red, and purple vertical reference lines indicate change points where reconstructed, SSP2-4.5 projected, and SSP5-8.5 projected runoff depths differ significantly ($p < 0.05$) based on the E-divisive method (Table S15 in Supporting Information S1).

both flood and extreme flood events increase significantly under the SSP5-8.5 scenario, with the frequency of extreme floods rising by approximately 50% compared to SSP2-4.5 (Table S14 in Supporting Information S1). The most severe hydrological drought and the most extreme flood event both occur under the SSP5-8.5 scenario, the former in 2048, with a RD more than 46% below the reconstructed mean, and the latter in 2094, with a RD more than 72% above the reconstructed mean (Figure 2f). These findings suggest that, regardless of the scenario, the RD in the CCWT will decline through the mid-century, accompanied by extreme drought events. However, by the end of the century, only under SSP5-8.5 would there be a rapid linear increase in RD along with a high frequency of extreme flood events.

3.2. Water Supply Variability and Extreme Events in the Pacific Rim Water Towers

The RD reconstruction for the Pacific Rim water towers explains 41.5%–82.3% of the variance of the observations, including the calculated first-order difference (Figure S5 in Supporting Information S1). This indicates the good performance of the reconstruction, and that the multi-model integrated reconstruction captures the interannual to decadal signals of hydrological changes, providing valuable information for runoff evaluation (Figure S9 in Supporting Information S1). Spatially, the reconstructed runoff depths of these water towers have statistically significant ($p < 0.05$) positive correlations with the observed data over the regions encompassing the major headwaters or upstream runoff production zones of major continental rivers (Figure 1a). However, the discrepancies and uncertainties between the reconstructed and observed RD cannot be overlooked. In terms of low-frequency signal simulation, the reconstructions for CCWT, Mongolian Plateau, and CA fail to adequately capture the observed wet and dry periods (Figure S5 in Supporting Information S1). In addition, the analysis based on first-order differencing indicates that some water towers also show limitations in simulating extreme flood and drought events. This is especially true for CA, where the drought atlas failed to accurately capture most observed hydrological events during the validation period (1950–2000) (Figure S5 in Supporting Information S1). These discrepancies may reflect the inherent limitations of proxy records in reconstructing extreme hydrological conditions (Ballesteros-Cánovas et al., 2015; Briffa et al., 1996; Esper & Frank, 2009). Our analysis reveals that on the western Pacific Rim, excluding the TP, the density distributions of reconstructed, observed, and scenario-projected runoff depths have relatively stable characteristics (Figure S10 in Supporting Information S1). Specifically, the distributions of the CCWT and Mongolian Plateau are approximately symmetrical and centered around the mean, with the interquartile range (25%–75%) showing minor fluctuations across different periods. However, extreme values are observed, such as in the GDR, where both the observed and reconstructed historical periods show frequent extremes, and the SSP2-4.5 projected results are markedly dispersed. In contrast, the density distributions of the TP and the eastern Pacific water towers exhibit multimodal patterns with inconsistent skewness directions: the TP and CA show an increased right skewness, while the NR exhibit left-skewed distributions. These density curves are broader, with high data dispersion, reflecting strong variability.

Analyses of the recurrence interval of extreme hydrological events indicate that warming scenarios make high-latitude and high-altitude river source areas in the Pacific Rim more prone to frequent extreme events (Figures 3a and 3b and Figure S11 in Supporting Information S1). The CCWT exhibits a decreasing frequency of extreme events over time, reflecting increasingly stable hydrological patterns. The Mongolian Plateau experienced extreme events every 10–20 years during 1700–1800 CE and post-1900, with the earlier periods dominated by extreme floods and later periods characterized by the dual hazards of floods and droughts. The TP shows the highest frequency of extreme flood events among all the water towers, especially since 1950, when such events have occurred every 5 years. This trend likely reflects enhanced glacial meltwater contributions driven by climatic warming (F. Chen et al., 2023). The frequency of extreme drought events in the GDR has remained relatively stable, but extreme flood events have gradually increased since 1900. Similarly, the NR, like the TP, shows an increasing frequency of extreme events, but with the dominance of hydrological droughts occurring every 6–10 years since 1950. The SR have consistently exhibited high-frequency extreme events at ∼20-year intervals, except during 1650–1700 CE. Lastly, the CA displayed relatively stable conditions during 1750–1900 CE; however, since 1950, the combined effects of hydrological droughts and floods have increased the frequency of extreme events to intervals shorter than 10–20 years. If the long-term mean is used as the classification threshold and the joint return period is estimated based on the duration and mean intensity of events (Hessl et al., 2018), the results show that CCWT and NR did not experience any extreme mega-droughts or pluvial periods (≥450 years) within the reconstructed time frame (Figures 3c and 3d and Figure S12 in Supporting Information S1). In contrast, other Pacific Rim water towers experienced such rare hydrological disasters. However, over shorter joint return periods

(<100 years), the count of drought and pluvial periods in CCWT was significantly higher than in other water towers. It should be noted that these periods are mostly of shorter duration (1–2 years) and moderate mean severity (falling within the 20th to 80th percentile range) (Figure 2f and Figure S12 in Supporting Information S1). This may be due to the fact that the monsoon system produces larger short-term disturbances to the RD variability in CCWT, while the background climate conditions in the Qinling-Daba Mountains may be more stable, resulting in a strong ability to recover to long-term conditions in a relatively short time (Davis et al., 2019; Ding, 1992). Meanwhile, we observe that the frequency distribution of joint return periods for droughts and pluvials in CCWT is approximately symmetric, whereas other water towers do not exhibit a similar pattern (Figures 3c and 3d). This pattern may indicate that the hydrological cycle in CCWT is relatively balanced, without a significant tendency toward either extreme event type.

3.3. Long-Term Trends and Stability Characteristics of Water Supply in the Pacific Rim Water Towers

Longer, more dependable, and spatially consistent proxy data are essential for analyzing the long-term trends in RD of these water towers (Smerdon et al., 2023). We extended the reconstructed and projected runoff depths for all water towers using a 40-year backward moving window to directly compare their trends with the mean state of the observational data (Figure 4a). The results indicate that, unlike other water towers, the CCWT exhibits a stable long-term trend. Only under high-emission scenarios (SSP5-8.5) are two brief but significant fluctuations observed: a decline in the mid-21st century and an increase at the end of the century. The only three change points identified by the E-divisive analysis are all within the SSP5-8.5 projection period, occurring in 2014, 2037, and 2058 (Table S15 in Supporting Information S1). For most other periods, the CCWT maintains a stable fluctuation range, suggesting that its RD remains within the limits of natural variability during both historical periods and under sustainable development scenarios (SSP2-4.5). Conversely, other water towers display significant deviations from their natural states over the long term. For example, the Mongolian Plateau experienced a short drought period during ∼1650–1700 CE and a prolonged wet period in ∼1,800, both exceeding the 95% CI estimated by regionalized approaches, supported by significant p-values and change points (Figure 4b). The TP exhibits the most pronounced fluctuations among all Pacific Rim water towers, consistently exceeding confidence levels during both the reconstructed and projected periods (Figure 4c). All the change points appeared after 1,880, with a notable increase in the frequency of hydrological shifts after 1990. These results indicate that the hydrological trends currently observed in TP are unprecedented, and model projections give worse expectations than existing observations. Even under the path of sustainable development, irreversible water loss in the TP is inevitable. The GDR experienced several historical drought periods that deviate from modern observational data. However, model projections suggest that hydrological fluctuations in the GDR almost remain within current observational levels throughout the 21st century (Figure 4d).

In contrast, the North and South American water towers (NR, SR, CA) exhibit minimal deviations in historical runoff variations compared to modern observations, indicating general stability. Among them, the historical water supply status of North America water towers is the most stable compared with modern observation records. Although there are five change points in the CA Mountains in South America that exceed the 95% confidence test, showing a turning point in trend change, most of the fluctuations are within the variability set by modern observation records. Model projections, however, suggest significant non-stationarity for these regions. For the NR, since 1937, water supply has been declining, and a substantial and rapid decline is projected under both scenarios throughout the 21st century, surpassing the magnitude and rate of change observed over the past 400 years (Figure 4e, Table S15 in Supporting Information S1). The reasons behind this projected trend are likely multifaceted and complex. Factors such as reduced snow and ice melt, changes in precipitation patterns, increased evapotranspiration, more frequent extreme drought events, and the historical reference background are all indispensable contributors (B. I. Cook et al., 2020). The future runoff projections for the SR and CA exhibit a trend similar to that of CCWT and Mongolian Plateau, characterized by a long-term decline to a critical threshold followed by a subsequent increase. Among them, the SR show the most pronounced changes under the SSP5-8.5 scenario, where the lowest 40-year moving average within the three detected change points (2016–2070) is nearly three times lower than the past 400 years. Even under the SSP2-4.5 scenario, the SR deviates from its long-term stable state, indicating that, even if a middle-of-the-road socio-economic development pathway is maintained, most of the North American west coast will still face a long-term drying trend and the risk of departing from its natural hydrological state. The projection of the long-term trend in RD for CA indicates that by the 2060s, the RD

under both scenarios will exceed the long-term state observed in modern records and historical reconstructions, maintaining a stable high-runoff output pattern.

3.4. Insights From the Reconstruction and Projection of Water Supply in the Pacific Rim Water Towers

By producing high-resolution RD reconstructions spanning multiple centuries, we systematically evaluated the historical hydrological variability, frequency of extreme events, and nonstationarity in future trends across Pacific Rim water towers. Among these, the CCWT exhibited the most stable water supply capacity, demonstrating strong internal regulatory and buffering capabilities. Several other water towers (NR, SR, CA) also exhibited long-term hydrological stability during the historical period (Figures 3 and 4). However, this stability was intermittently disrupted by short-term extreme hydrological events, likely driven by interannual to decadal climate variability, including the Pacific Decadal Oscillation and El Niño–Southern Oscillation (ENSO) (Barlow et al., 2001; Castino et al., 2017; Wallace & Minder, 2021). Moreover, under future high-emission scenarios, model projections indicate that these regions are likely to undergo significant departures from their natural variability range, suggesting an increased risk of hydrological extremes. Notably, the NR is the only water tower projected to exhibit a persistent decline in water supply capacity. This may reflect a consistent signal across Global Climate Models (GCMs) that forecast more intense warming and enhanced evapotranspiration in the region, leading to shortened snow cover duration, reduced soil moisture retention, and ultimately diminished effective runoff (B. I. Cook et al., 2020; Siirila-Woodburn et al., 2021). The Mongolian Plateau, GDR, and TP all demonstrated unstable patterns in terms of frequency, magnitude, and trends of extreme hydrological events during the historical period. However, the driving mechanisms behind these instabilities differ fundamentally. The GDR irregular precipitation patterns are dominantly modulated by ENSO (Higgins et al., 2022), while the Mongolian Plateau is affected by the eastward shift of the westerlies and the Siberian High (Cai et al., 2024). In contrast, the TP reflects an amplified response to modern climate warming in high-altitude regions, making recent warming the dominant driver of its persistent instability throughout the full time span (Hu et al., 2025; Yao et al., 2022). These divergent evolutionary pathways among the water towers indicate that simplified or homogenized climate response models are insufficient to capture their future trajectories (Collins et al., 2012). The hydrological processes of the CCWT are relatively stable, making it suitable to enhance system resilience through strengthened surface–groundwater coordination, improved ecological water retention capacity, and flexible regulation mechanisms. Conversely, the NR is projected to experience a persistent decline in water supply in the future, calling for strategies that focus on restoring snow-dependent hydrological systems, improving water-use efficiency, and promoting basin-scale cooperative governance. Effective future water resource management thus requires not only more refined projections, but also the implementation of differentiated regulation strategies and adaptive governance frameworks tailored to local conditions (Cosgrove & Loucks, 2015).

Despite the successful integration of proxy records and model data to assess the water supply capacity of the Pacific Rim water towers, several unavoidable sources of uncertainty remain. For instance, tree-ring proxy records may still be influenced by ecological processes and are limited in capturing extreme flood events (Ballesteros-Cánovas et al., 2015). Similarly, widely used drought atlases may not adequately capture hydroclimatic signals across the full hydrological year, particularly those associated with the cool season (Guo et al., 2025), as the target variable is a compromise for highly varying hydrological conditions and processes across space. Even though the drought atlases offer the convenience of not requiring detrending and standardization and outputting indicators on a large scale and gridding, its essence is still a data product after a series of regression operations (Nguyen et al., 2020). Further use is bound to result in error transmission and superposition. Therefore, reconstructions of pre-instrumental variability at a single site or small-scale watershed should be used with caution. The reliability and continuity of hydrological data also introduce potential errors (Ghiggi et al., 2019). Employed a hybrid approach combining station observations with gridded data sets to mitigate this, reconstruction accuracy may still be affected. More critically, the runoff trends simulated by CMIP6 models often diverge significantly from those inferred from historical reconstructions (Figure 2f and Figure S9 in Supporting Information S1), highlighting a series of structural and process-based uncertainties inherent in GCMs. These include differences in how models simulate key land surface hydrological processes, represent the climate system, and respond to radiative forcing from greenhouse gases and aerosols (Miao et al., 2023; Stouffer et al., 2017). Such discrepancies can lead to divergent assessments of future precipitation trends and extremes. Additionally, the multi-model ensemble means and bias correction methods may also inadvertently obscure true variability and potential nonstationarities (A. Wang et al., 2022). Therefore, future research should prioritize the use of multi-source

coupled simulation frameworks to enhance confidence in projecting mountain water tower evolution (Lehner et al., 2019), while also interpreting projection outcomes with greater caution given the underlying uncertainties. Nonetheless, our findings demonstrate that integrating paleo-hydrological reconstructions with climate model projections can provide an essential knowledge foundation for future adaptation efforts.

Conflict of Interest

The authors declare no conflicts of interest relevant to this study.

Data Availability Statement

The runoff depth reconstruction of Central China water tower can be downloaded from the Mendeley Data platform (https://data.mendeley.com/datasets/wh5g9hwv5g/1) (Yue & Chen, 2025). The drought atlas is available from the Tree-Ring Drought Atlas Portal website (http://drought.memphis.edu/). The China Natural Runoff Dataset version 1.0 (CNRDv1.0) can be downloaded from the National Tibetan Plateau/Third Pole Environment Data Center (https://www.tpdc.ac.cn/zh-hans/data/8b6a12c7-c8f9-465a-b449-852fbff51853/) (Miao & Gou, 2022). The CMIP6 data sets are accessible at Earth System Grid Federation website (https://esgf-node.llnl.gov/search/cmip6/). The observed CRU TS 4.08 gridded temperature and precipitation data can be accessed at the Climatic Research Unit (University of East Anglia) and Met Office (https://crudata.uea.ac.uk/cru/data/hrg/cru_ts_4.08/) (Harris et al., 2020). The Self-calibrating Palmer Drought Severity Index (scPDSI) gridded data set can be downloaded from the Climatic Research Unit (University of East Anglia) (https://crudata.uea.ac.uk/cru/data/drought/) (van der Schrier et al., 2013). The G-RUN gridded data set can be downloaded from the figshare website (https://figshare.com/articles/dataset/G-RUN_ENSEMBLE/12794075) (Ghiggi, Humphrey, Gudmundsson, & Seneviratne, 2021). Other observed hydrological data for reference and comparison come from the Global Runoff Data Centre (Global Runoff Data Center) (https://portal.grdc.bafg.de/applications/public.html?publicuser=PublicUser#dataDownload/Home).

Acknowledgments

This study was supported by the Excellent Research Group Program for Tibetan Plateau Earth System (42588201), the Natural Science Foundation of China (32061123008), the China Scholarship Council (202407030045), and the Scientific Research and Innovation Project of Postgraduate Students in the Academic Degree of Yunnan University (KC-23233869). We are deeply grateful to the pioneers and colleagues in dendrochronology who have devoted their efforts to collecting, analyzing, and sharing tree-ring data. Their open data contributions have laid a critical foundation for advancing research in climate–growth relationships and made this study possible. We sincerely thank Prof. Amy Hessl, Prof. Mariano S. Morales and Dr. Mukund Palat Rao for their invaluable code support, which inspired the manuscript writing process. We would like to express our sincere gratitude to the editor and the reviewers for their thoughtful comments and constructive suggestions, which have greatly improved the quality and clarity of this manuscript. Their professional insights and careful evaluations were invaluable in refining our analyses and interpretations.

References

An, W., Li, J., Wang, S., Xu, C., Shao, X., Qin, N., & Guo, Z. (2022). Hydrological extremes in the upper Yangtze River over the past 700 yr inferred from a tree ring $\delta_{18}O$ record. *Journal of Geophysical Research: Atmospheres*, *127*(10), e2021JD036109. https://doi.org/10.1029/2021JD036109

Ballesteros-Cánovas, J. A., Stoffel, M., St George, S., & Hirschboeck, K. (2015). A review of flood records from tree rings. *Progress in Physical Geography*, *39*(6), 794–816. https://doi.org/10.1177/0309133315608758

Barlow, M., Nigam, S., & Berbery, E. H. (2001). ENSO, Pacific decadal variability, and US summertime precipitation, drought, and stream flow. *Journal of Climate*, *14*(9), 2105–2128. https://doi.org/10.1175/1520-0442(2001)014<2105:EPDVAU>2.0.CO;2

Batista, G. E. A. P. A., Prati, R. C., & Monard, M. C. (2004). A study of the behavior of several methods for balancing machine learning training data. *ACM SIGKDD Explorations Newsletter*, *6*(1), 20–29. https://doi.org/10.1145/1007730.1007735

Biau, G., & Scornet, E. (2016). A random forest guided tour. *TEST*, *25*(2), 197–227. https://doi.org/10.1007/s11749-016-0481-7

Briffa, K. R., Jones, P. D., Schweingruber, F. H., Karlén, W., & Shiyatov, S. G. (1996). Tree-ring variables as proxy-climate indicators: Problems with low-frequency signals. In *Climatic variations and forcing mechanisms of the last 2000 years* (pp. 9–41). Springer Berlin Heidelberg. https://doi.org/10.1007/978-3-642-61113-1_2

Cai, Q., Chen, W., Chen, S., Xie, S. P., Piao, J., Ma, T., & Lan, X. (2024). Recent pronounced warming on the Mongolian Plateau boosted by internal climate variability. *Nature Geoscience*, *17*(3), 181–188. https://doi.org/10.1038/s41561-024-01377-6

Cao, H., Chen, F., Hu, M., Hou, T., Zhao, X., Wang, S., et al. (2025). Tree-ring insights into past and future streamflow variations in Beijing, northern China. *Water Resources Research*, *61*(1). e2024WR038084. https://doi.org/10.1029/2024wr038084

Castino, F., Bookhagen, B., & Strecker, M. R. (2017). Oscillations and trends of river discharge in the southern Central Andes and linkages with climate variability. *Journal of Hydrology*, *555*, 108–124. https://doi.org/10.1016/j.jhydrol.2017.10.001

Chen, F., Man, W., Wang, S., Esper, J., Meko, D., Büntgen, U., et al. (2023). Southeast Asian ecological dependency on Tibetan Plateau streamflow over the last millennium. *Nature Geoscience*, *16*(12), 1151–1158. https://doi.org/10.1038/s41561-023-01320-1

Chen, F., Shang, H., Panyushkina, I., Meko, D. M., Li, J., Yuan, Y., et al. (2019a). 500-year tree-ring reconstruction of Salween River streamflow related to the history of water supply in Southeast Asia. *Climate Dynamics*, *53*(11), 6595–6607. https://doi.org/10.1007/s00382-019-04948-1

Chen, F., Shang, H., Panyushkina, I. P., Meko, D. M., Yu, S., Yuan, Y., et al. (2019b). Tree-ring reconstruction of Lhasa River streamflow reveals 472 years of hydrologic change on southern Tibetan Plateau. *Journal of Hydrology*, *572*, 169–178. https://doi.org/10.1016/j.jhydrol.2019.02.054

Chen, F., Wang, S., Dong, Q., Esper, J., Büntgen, U., Meko, D., et al. (2024). Role of Pacific Ocean climate in regulating runoff in the source areas of water transfer projects on the Pacific Rim. *npj Climate and Atmospheric Science*, *7*(1), 153. https://doi.org/10.1038/s41612-024-00706-1

Chen, F., Wang, T., Zhao, X., Esper, J., Ljungqvist, F. C., Büntgen, U., et al. (2024). Coupled Pacific Rim megadroughts contributed to the fall of the Ming Dynasty's capital in 1644 CE. *Science Bulletin*, *69*(19), 3106–3114. https://doi.org/10.1016/j.scib.2024.04.029

Chen, S. X., & Huang, T. M. (2007). Nonparametric estimation of copula functions for dependence modelling. *Canadian Journal of Statistics*, *35*(2), 265–282. https://doi.org/10.1002/cjs.5550350205

Chen, T. (2015). Xgboost: Extreme gradient boosting. *R package version 0.4-2*, *1*(4).

Cleaveland, M. K. (2000). A 963-year reconstruction of summer (JJA) stream flow in the White River, Arkansas, USA, from tree-rings. *The Holocene*, *10*(1), 33–41. https://doi.org/10.1191/095968300666157027

Cleveland, W. S., & Devlin, S. J. (1988). Locally weighted regression: An approach to regression analysis by local fitting. *Journal of the American Statistical Association*, *83*(403), 596–610. https://doi.org/10.1080/01621459.1988.10478639
Collins, M., Chandler, R. E., Cox, P. M., Huthnance, J. M., Rougier, J., & Stephenson, D. B. (2012). Quantifying future climate change. *Nature Climate Change*, *2*(6), 403–409. https://doi.org/10.1038/nclimate1414
Cook, B. I., Mankin, J. S., Marvel, K., Williams, A. P., Smerdon, J. E., & Anchukaitis, K. J. (2020). Twenty-first century drought projections in the CMIP6 forcing scenarios. *Earth's Future*, *8*(6), e2019EF001461. https://doi.org/10.1029/2019EF001461
Cook, E. R., Anchukaitis, K. J., Buckley, B. M., D'Arrigo, R. D., Jacoby, G. C., & Wright, W. E. (2010). Asian monsoon failure and megadrought during the last millennium. *Science*, *328*(5977), 486–489. https://doi.org/10.1126/science.1185188
Cook, E. R., & Kairiukstis, L. A. (2013). *Methods of dendrochronology: Applications in the environmental sciences*. Springer. https://doi.org/10.1007/978-94-015-7879-0
Cook, E. R., Krusic, P. J., Anchukaitis, K. J., Buckley, B. M., Nakatsuka, T., Sano, M., et al. (2013). Tree-ring reconstructed summer temperature anomalies for temperate East Asia since 800 C.E. *Climate Dynamics*, *41*(11), 2957–2972. https://doi.org/10.1007/s00382-012-1611-x
Cook, E. R., Seager, R., Heim Jr, R. R., Vose, R. S., Herweijer, C., & Woodhouse, C. (2010). Megadroughts in North America: Placing IPCC projections of hydroclimatic change in a long-term palaeoclimate context. *Journal of Quaternary Science*, *25*(1), 48–61. https://doi.org/10.1002/jqs.1303
Cosgrove, W. J., & Loucks, D. P. (2015). Water management: Current and future challenges and research directions. *Water Resources Research*, *51*(6), 4823–4839. https://doi.org/10.1002/2014WR016869
Davis, K. T., Dobrowski, S. Z., Holden, Z. A., Higuera, P. E., & Abatzoglou, J. T. (2019). Microclimatic buffering in forests of the future: The role of local water balance. *Ecography*, *42*(1), 1–11. https://doi.org/10.1111/ecog.03836
Deng, Y., Gou, X., Gao, L., Yang, T., & Yang, M. (2014). Early-summer temperature variations over the past 563 yr inferred from tree rings in the Shaluli Mountains, southeastern Tibet Plateau. *Quaternary Research*, *81*(3), 513–519. https://doi.org/10.1016/j.yqres.2013.08.002
Ding, Y. (1992). Summer monsoon rainfalls in China. *Journal of the Meteorological Society of Japan. Ser. II*, *70*(1B), 373–396. https://doi.org/10.2151/jmsj1965.70.1B_373
Do, H. X., Gudmundsson, L., Leonard, M., & Westra, S. (2018). The Global Streamflow Indices and Metadata Archive (GSIM)—Part 1: The production of a daily streamflow archive and metadata. *Earth System Science Data*, *10*(2), 765–785. https://doi.org/10.5194/essd-10-765-2018
Esper, J., & Frank, D. (2009). Divergence pitfalls in tree-ring research. *Climatic Change*, *94*(3), 261–266. https://doi.org/10.1007/s10584-009-9594-2
Esper, J., Torbenson, M., & Büntgen, U. (2024). 2023 summer warmth unparalleled over the past 2,000 years. *Nature*, *631*(8019), 94–97. https://doi.org/10.1038/s41586-024-07512-y
Eyring, V., Bony, S., Meehl, G. A., Senior, C. A., Stevens, B., Stouffer, R. J., & Taylor, K. E. (2016). Overview of the Coupled Model Intercomparison Project Phase 6 (CMIP6) experimental design and organization. *Geoscientific Model Development*, *9*(5), 1937–1958. https://doi.org/10.5194/gmd-9-1937-2016
Fang, K., Gou, X., Chen, F., D'Arrigo, R., & Li, J. (2010). Tree-ring based drought reconstruction for the Guiqing Mountain (China): Linkages to the Indian and Pacific Oceans. *International Journal of Climatology*, *30*(8), 1137–1145. https://doi.org/10.1002/joc.1974
Gao, L., Deng, Y., Yan, X., Li, Q., Zhang, Y., & Gou, X. (2021). The unusual recent streamflow declines in the Bailong River, north-central China, from a multi-century perspective. *Quaternary Science Reviews*, *260*, 106927. https://doi.org/10.1016/j.quascirev.2021.106927
Ghiggi, G., Humphrey, V., Gudmundsson, L., & Seneviratne, S. I. (2021). G-RUN ENSEMBLE (Version 1). *figshare*. https://doi.org/10.6084/m9.figshare.12794075.v1
Ghiggi, G., Humphrey, V., Seneviratne, S. I., & Gudmundsson, L. (2019). GRUN: An observation-based global gridded runoff dataset from 1902 to 2014. *Earth System Science Data*, *11*(4), 1655–1674. https://doi.org/10.5194/essd-11-1655-2019
Ghiggi, G., Humphrey, V., Seneviratne, S. I., & Gudmundsson, L. (2021). G-RUN ENSEMBLE: A multi-forcing observation-based global runoff reanalysis. *Water Resources Research*, *57*(5), e2020WR028787. https://doi.org/10.1029/2020WR028787
Gou, J., Miao, C., Samaniego, L., Xiao, M., Wu, J., & Guo, X. (2021). CNRD v1.0: A high-quality natural runoff dataset for hydrological and climate studies in China. *Bulletin of the American Meteorological Society*, *102*(5), E929–E947. https://doi.org/10.1175/BAMS-D-20-0094.1
Gou, X., Deng, Y., Chen, F., Yang, M., Fang, K., Gao, L., et al. (2010). Tree ring based streamflow reconstruction for the Upper Yellow River over the past 1234 years. *Chinese Science Bulletin*, *55*(36), 4179–4186. https://doi.org/10.1007/s11434-010-4215-z
Gudmundsson, L., Do, H. X., Leonard, M., & Westra, S. (2018). The Global Streamflow Indices and Metadata Archive (GSIM)–Part 2: Quality control, time-series indices and homogeneity assessment. *Earth System Science Data*, *10*(2), 787–804. https://doi.org/10.5194/essd-10-787-2018
Guo, R., Nguyen, H. T., Galelli, S., Ceola, S., & Montanari, A. (2025). Bridging information from paleo-hydrological and climate model ensembles to assess long term hydrological drought hazard. *AGU Advances*, *6*(2), e2024AV001393. https://doi.org/10.1029/2024AV001393
Hadad, M. A., González-Reyes, Á., Roig, F. A., Matskovsky, V., & Cherubini, P. (2021). Tree-ring-based hydroclimatic reconstruction for the northwest Argentine Patagonia since 1055 CE and its teleconnection to large-scale atmospheric circulation. *Global and Planetary Change*, *202*, 103496. https://doi.org/10.1016/j.gloplacha.2021.103496
Hans, C. (2011). Elastic net regression modeling with the orthant normal prior. *Journal of the American Statistical Association*, *106*(496), 1383–1393. https://doi.org/10.1198/jasa.2011.tm09241
Harris, I., Osborn, T. J., Jones, P., & Lister, D. (2020). Version 4 of the CRU TS monthly high-resolution gridded multivariate climate dataset. *Scientific Data*, *7*(1), 109. https://doi.org/10.1038/s41597-020-0453-3
Hessl, A. E., Anchukaitis, K. J., Jelsema, C., Cook, B., Byambasuren, O., Leland, C., et al. (2018). Past and future drought in Mongolia. *Science Advances*, *4*(3), e1701832. https://doi.org/10.1126/sciadv.1701832
Higgins, P. A., Palmer, J. G., Rao, M. P., Andersen, M. S., Turney, C. S., & Johnson, F. (2022). Unprecedented high Northern Australian streamflow linked to an intensification of the Indo-Australian Monsoon. *Water Resources Research*, *58*(3), e2021WR030881. https://doi.org/10.1029/2021WR030881
Hoegh-Guldberg, O., Jacob, D., Taylor, M., Guillén Bolaños, T., Bindi, M., Brown, S., et al. (2019). The human imperative of stabilizing global climate change at 1.5°C. *Science*, *365*(6459), eaaw6974. https://doi.org/10.1126/science.aaw6974
Homfeld, I. K., Büntgen, U., Reinig, F., Torbenson, M. C. A., & Esper, J. (2024). Application of RCS and signal-free RCS to tree-ring width and maximum latewood density data. *Dendrochronologia*, *85*, 126205. https://doi.org/10.1016/j.dendro.2024.126205
Hu, M., Zhao, X., Chen, F., Wang, S., Torbenson, M. C. A., Hou, T., & Chen, Y. (2025). Increasing evidence of an anthropogenic signal in drought variations on the river source areas of southeastern Tibetan Plateau.*Journal of Hydrology*, *660*, 133508. https://doi.org/10.1016/j.jhydrol.2025.133508
Islam, N., Vennemann, T., Büntgen, U., Cherubini, P., & Lane, S. N. (2024). Tree-ring hydrological research in the Himalaya: State of the art and future directions. *Progress in Physical Geography: Earth and Environment*, *48*(3), 454–489. https://doi.org/10.1177/03091333241229919

Karl, T. R., & Trenberth, K. E. (2003). Modern global climate change. *Science*, *302*(5651), 1719–1723. https://doi.org/10.1126/science.1090228
Lehner, F., Wood, A. W., Vano, J. A., Lawrence, D. M., Clark, M. P., & Mankin, J. S. (2019). The potential to reduce uncertainty in regional runoff projections from climate models. *Nature Climate Change*, *9*(12), 926–933. https://doi.org/10.1038/s41558-019-0639-x
Li, T., Lan, T., Zhang, H., Sun, J., Xu, C. Y., & David Chen, Y. (2024). Identifying the possible driving mechanisms in Precipitation-Runoff relationships with nonstationary and nonlinear theory approaches. *Journal of Hydrology*, *639*, 131535. https://doi.org/10.1016/j.jhydrol.2024.131535
Liu, N., Bao, G., Liu, Y., & Linderholm, H. W. (2019). Two centuries-long streamflow reconstruction inferred from tree rings for the middle reaches of the Weihe River in Central China. *Forests*, *10*(3), 208. https://doi.org/10.3390/f10030208
Liu, Y., Song, H., An, Z., Sun, C., Trouet, V., Cai, Q., et al. (2020). Recent anthropogenic curtailing of Yellow River runoff and sediment load is unprecedented over the past 500 y. *Proceedings of the National Academy of Sciences*, *117*(31), 18251–18257. https://doi.org/10.1073/pnas.1922349117
Ljungqvist, F. C., Piermattei, A., Seim, A., Krusic, P. J., Büntgen, U., He, M., et al. (2020). Ranking of tree-ring based hydroclimate reconstructions of the past millennium. *Quaternary Science Reviews*, *230*, 106074. https://doi.org/10.1016/j.quascirev.2019.106074
Marquardt, D. W., & Snee, R. D. (1975). Ridge regression in practice. *The American Statistician*, *29*(1), 3–20. https://doi.org/10.1080/00031305.1975.10479105
Martin, J. T., Pederson, G. T., Woodhouse, C. A., Cook, E. R., McCabe, G. J., Wise, E. K., et al. (2019). 1200 years of Upper Missouri River streamflow reconstructed from tree rings. *Quaternary Science Reviews*, *224*, 105971. https://doi.org/10.1016/j.quascirev.2019.105971
Matteson, D. S., & James, N. A. (2014). A nonparametric approach for multiple change point analysis of multivariate data. *Journal of the American Statistical Association*, *109*(505), 334–345. https://doi.org/10.1080/01621459.2013.849605
Maxwell, R. S., Harley, G. L., Maxwell, J. T., Rayback, S. A., Pederson, N., Cook, E. R., et al. (2017). An interbasin comparison of tree-ring reconstructed streamflow in the eastern United States. *Hydrological Processes*, *31*(13), 2381–2394. https://doi.org/10.1002/hyp.11188
McDonald, G. C. (2009). Ridge regression. *WIREs Computational Statistics*, *1*(1), 93–100. https://doi.org/10.1002/wics.14
McPartland, M. Y., St. George, S., Pederson, G. T., & Anchukaitis, K. J. (2020). Does signal-free detrending increase chronology coherence in large tree-ring networks? *Dendrochronologia*, *63*, 125755. https://doi.org/10.1016/j.dendro.2020.125755
Meko, D. M., Therrell, M. D., Baisan, C. H., & Hughes, M. K. (2001). Sacramento river flow reconstructed to A.D. 869 from tree rings. *JAWRA Journal of the American Water Resources Association*, *37*(4), 1029–1039. https://doi.org/10.1111/j.1752-1688.2001.tb05530.x
Meko, D. M., Woodhouse, C. A., & Winitsky, A. G. (2022). Tree-Ring perspectives on the Colorado River: Looking back and moving forward. *JAWRA Journal of the American Water Resources Association*, *58*(5), 604–621. https://doi.org/10.1111/1752-1688.12989
Miao, C., & Gou, J. (2022). CNRDv1.0: The China natural runoff dataset version 1.0 (1961–2018) (version 1.0) [Dataset]. *National Tibetan Plateau / Third Pole Environment Data Center*. https://doi.org/10.11888/Atmos.tpdc.272864
Miao, C., Gou, J., Fu, B., Tang, Q., Duan, Q., Chen, Z., et al. (2022). High-quality reconstruction of China's natural streamflow. *Science Bulletin*, *67*(5), 547–556. https://doi.org/10.1016/j.scib.2021.09.022
Miao, C., Gou, J., Hu, J., & Duan, Q. (2024). Impacts of different satellite-based precipitation signature errors on hydrological modeling performance across China. *Earth's Future*, *12*(11), e2024EF004954. https://doi.org/10.1029/2024EF004954
Miao, C., Wu, Y., Fan, X., & Su, J. (2023). Projections of global land runoff changes and their uncertainty characteristics during the 21st century. *Earth's Future*, *11*(4), e2022EF003286. https://doi.org/10.1029/2022EF003286
Montgomery, D. C., Peck, E. A., & Vining, G. G. (2021). *Introduction to linear regression analysis*. Wiley.
Moore, R. J., & Clarke, R. T. (1981). A distribution function approach to rainfall runoff modeling. *Water Resources Research*, *17*(5), 1367–1382. https://doi.org/10.1029/WR017i005p01367
Morales, M. S., Cook, E. R., Barichivich, J., Christie, D. A., Villalba, R., LeQuesne, C., et al. (2020). Six hundred years of South American tree rings reveal an increase in severe hydroclimatic events since mid-20th century. *Proceedings of the National Academy of Sciences*, *117*(29), 16816–16823. https://doi.org/10.1073/pnas.2002411117
Morales, M. S., Crispín-DelaCruz, D. B., Álvarez, C., Christie, D. A., Ferrero, M. E., Andreu-Hayles, L., et al. (2023). Drought increase since the mid-20th century in the northern South American Altiplano revealed by a 389-year precipitation record. *Climate of the Past*, *19*(2), 457–476. https://doi.org/10.5194/cp-19-457-2023
Mudelsee, M. (2014). *Climate time series analysis: Classical statistical and bootstrap methods*. Springer. https://doi.org/10.1007/978-3-319-04450-7
Muñoz, A. A., González-Reyes, A., Lara, A., Sauchyn, D., Christie, D., Puchi, P., et al. (2016). Streamflow variability in the Chilean Temperate-Mediterranean climate transition (35°S–42°S) during the last 400 years inferred from tree-ring records. *Climate Dynamics*, *47*(12), 4051–4066. https://doi.org/10.1007/s00382-016-3068-9
Natekin, A., & Knoll, A. (2013). Gradient boosting machines, a tutorial. *Frontiers in Neurorobotics*, *7*, 21. https://doi.org/10.3389/fnbot.2013.00021
Nguyen, H. T. T., Turner, S. W. D., Buckley, B. M., & Galelli, S. (2020). Coherent streamflow variability in monsoon Asia over the past eight Centuries—Links to Oceanic drivers. *Water Resources Research*, *56*(12), e2020WR027883. https://doi.org/10.1029/2020WR027883
Noguchi, K., Gel, Y. R., & Duguay, C. R. (2011). Bootstrap-based tests for trends in hydrological time series, with application to ice phenology data. *Journal of Hydrology*, *410*(3), 150–161. https://doi.org/10.1016/j.jhydrol.2011.09.008
PAGES Hydro2k Consortium. (2017). Comparing proxy and model estimates of hydroclimate variability and change over the Common era. *Climate of the Past*, *13*(12), 1851–1900. https://doi.org/10.5194/cp-13-1851-2017
Palmer, J. G., Cook, E. R., Turney, C. S., Allen, K., Fenwick, P., Cook, B. I., et al. (2015). Drought variability in the eastern Australia and New Zealand summer drought atlas (ANZDA, CE 1500–2012) modulated by the Interdecadal Pacific Oscillation. *Environmental Research Letters*, *10*(12), 124002. https://doi.org/10.1088/1748-9326/10/12/124002
Porporato, A., & Ridolfi, L. (1997). Nonlinear analysis of river flow time sequences. *Water Resources Research*, *33*(6), 1353–1367. https://doi.org/10.1029/96WR03535
Ranstam, J., & Cook, J. A. (2018). LASSO regression. *British Journal of Surgery*, *105*(10), 1348. https://doi.org/10.1002/bjs.10895
Rao, M. P., Cook, E. R., Cook, B. I., D'Arrigo, R. D., Palmer, J. G., Lall, U., et al. (2020). Seven centuries of reconstructed Brahmaputra River discharge demonstrate underestimated high discharge and flood hazard frequency. *Nature Communications*, *11*(1), 6017. https://doi.org/10.1038/s41467-020-19795-6
Razavi, S., Elshorbagy, A., Wheater, H., & Sauchyn, D. (2015). Toward understanding nonstationarity in climate and hydrology through tree ring proxy records. *Water Resources Research*, *51*(3), 1813–1830. https://doi.org/10.1002/2014WR015696
Rigatti, S. J. (2017). Random Forest. *Journal of Insurance Medicine*, *47*(1), 31–39. https://doi.org/10.17849/insm-47-01-31-39.1

Siirila-Woodburn, E. R., Rhoades, A. M., Hatchett, B. J., Huning, L. S., Szinai, J., Tague, C., et al. (2021). A low-to-no snow future and its impacts on water resources in the western United States. *Nature Reviews Earth & Environment*, *2*(11), 800–819. https://doi.org/10.1038/s43017-021-00219-y

Sklar, A. (1973). Random variables, joint distribution functions, and copulas. *Kybernetika*, *9*(6), 449–460. Retrieved from http://eudml.org/doc/28992

Smerdon, J. E., Cook, E. R., & Steiger, N. J. (2023). The historical development of large-scale paleoclimate field reconstructions over the common era. *Reviews of Geophysics*, *61*(4), e2022RG000782. https://doi.org/10.1029/2022RG000782

Smith, A. J., Donovan, J. J., Ito, E., Engstrom, D. R., & Panek, V. A. (2002). Climate-driven hydrologic transients in lake sediment records: Multiproxy record of mid-holocene drought. *Quaternary Science Reviews*, *21*(4), 625–646. https://doi.org/10.1016/S0277-3791(01)00041-5

Sorg, A., Bolch, T., Stoffel, M., Solomina, O., & Beniston, M. (2012). Climate change impacts on glaciers and runoff in Tien Shan (Central Asia). *Nature Climate Change*, *2*(10), 725–731. https://doi.org/10.1038/nclimate1592

Speer, J. H. (2010). *Fundamentals of tree-ring research*. University of Arizona Press.

Stouffer, R. J., Eyring, V., Meehl, G. A., Bony, S., Senior, C., Stevens, B., & Taylor, K. E. (2017). CMIP5 scientific gaps and recommendations for CMIP6. *Bulletin of the American Meteorological Society*, *98*(1), 95–105. https://doi.org/10.1175/BAMS-D-15-00013.1

Su, X., Yan, X., & Tsai, C. L. (2012). Linear regression. *WIREs Computational Statistics*, *4*(3), 275–294. https://doi.org/10.1002/wics.1198

Sun, C., & Liu, Y. (2019). Tree-ring-based drought variability in the eastern region of the Silk Road and its linkages to the Pacific Ocean. *Ecological Indicators*, *96*, 421–429. https://doi.org/10.1016/j.ecolind.2018.09.032

Sun, Q., Zhou, W. X., & Fan, J. (2020). Adaptive huber regression. *Journal of the American Statistical Association*, *115*(529), 254–265. https://doi.org/10.1080/01621459.2018.1543124

Torbenson, M. C. A., & Stagge, J. H. (2021). Informing seasonal proxy-based flow reconstructions using baseflow separation: An example from the Potomac River, United States. *Water Resources Research*, *57*(2), e2020WR027706. https://doi.org/10.1029/2020WR027706

Tozer, C. R., Vance, T. R., Roberts, J. L., Kiem, A. S., Curran, M. A. J., & Moy, A. D. (2016). An ice core derived 1013-year catchment-scale annual rainfall reconstruction in subtropical eastern Australia. *Hydrology and Earth System Sciences*, *20*(5), 1703–1717. https://doi.org/10.5194/hess-20-1703-2016

van der Schrier, G., Barichivich, J., Briffa, K. R., & Jones, P. D. (2013). A scPDSI-based global data set of dry and wet spells for 1901–2009. *Journal of Geophysical Research: Atmospheres*, *118*(10), 4025–4048. https://doi.org/10.1002/jgrd.50355

Viorica, N., Cătălin-Constantin, R., Andrei, M., Marian-Ionu, ., Ionel, P., & Monica, I. (2023). The first tree-ring reconstrruction of streamflow variability over the last ∼250 years in the Lower Danube. *Journal of Hydrology*, *617*, 129150. https://doi.org/10.1016/j.jhydrol.2023.129150

Viviroli, D., Archer, D. R., Buytaert, W., Fowler, H. J., Greenwood, G. B., Hamlet, A. F., et al. (2011). Climate change and mountain water resources: Overview and recommendations for research, management and policy. *Hydrology and Earth System Sciences*, *15*(2), 471–504. https://doi.org/10.5194/hess-15-471-2011

Viviroli, D., & Weingartner, R. (2004). The hydrological significance of mountains: From regional to global scale. *Hydrology and Earth System Sciences*, *8*(6), 1017–1030. https://doi.org/10.5194/hess-8-1017-2004

Vörösmarty, C. J., McIntyre, P. B., Gessner, M. O., Dudgeon, D., Prusevich, A., Green, P., et al. (2010). Global threats to human water security and river biodiversity. *Nature*, *467*(7315), 555–561. https://doi.org/10.1038/nature09440

Vuille, M., Carey, M., Huggel, C., Buytaert, W., Rabatel, A., Jacobsen, D., et al. (2018). Rapid decline of snow and ice in the tropical Andes – Impacts, uncertainties and challenges ahead. *Earth-Science Reviews*, *176*, 195–213. https://doi.org/10.1016/j.earscirev.2017.09.019

Wallace, B., & Minder, J. R. (2021). The impact of snow loss and soil moisture on convective precipitation over the Rocky Mountains under climate warming. *Climate Dynamics*, *56*(9), 2915–2939. https://doi.org/10.1007/s00382-020-05622-7

Wand, M. P., & Jones, M. C. (1994). *Kernel smoothing*. CRC Press.

Wang, A., Miao, Y., Kong, X., & Wu, H. (2022). Future changes in global runoff and runoff coefficient from CMIP6 multi-model simulation under SSP1-2.6 and SSP5-8.5 scenarios. *Earth's Future*, *10*(12), e2022EF002910. https://doi.org/10.1029/2022EF002910

Wang, X., Zhang, Y., Feng, X., Feng, Y., Xue, Y., & Pan, N. (2017). Analysis and application of drought characteristics based on run theory and Copula function. *Transactions of the Chinese Society of Agricultural Engineering*, *33*(10), 206–214. https://doi.org/10.11975/j.issn.1002-6819.2017.10.027

Williams, A. P., Cook, E. R., Smerdon, J. E., Cook, B. I., Abatzoglou, J. T., Bolles, K., et al. (2020). Large contribution from anthropogenic warming to an emerging North American megadrought. *Science*, *368*(6488), 314–318. https://doi.org/10.1126/science.aaz9600

Wohl, E. E. (2013). *Mountain rivers, 14*. American Geophysical Union. https://doi.org/10.1029/WM014

Woodhouse, C. A., & Lukas, J. J. (2006). Multi-Century tree-ring reconstructions of Colorado streamflow for water resource planning. *Climatic Change*, *78*(2), 293–315. https://doi.org/10.1007/s10584-006-9055-0

Wu, H., Fang, K., & Li, X. (2024). Examining the effect of sample size on the estimation of low-frequency signals in tree-ring chronologies. *Dendrochronologia*, *85*, 126213. https://doi.org/10.1016/j.dendro.2024.126213

Wu, L., Zhang, X., Hao, F., Wu, Y., Li, C., & Xu, Y. (2020). Evaluating the contributions of climate change and human activities to runoff in typical semi-arid area, China. *Journal of Hydrology*, *590*, 125555. https://doi.org/10.1016/j.jhydrol.2020.125555

Wu, R., Zhang, J., Bao, Y., & Guo, E. (2019). Run theory and copula-based drought risk analysis for songnen grassland in Northeastern China. *Sustainability*, *11*(21), 6032. https://doi.org/10.3390/su11216032

Wu, Y., Gan, T. Y., She, Y., Xu, C., & Yan, H. (2020). Five centuries of reconstructed streamflow in Athabasca River Basin, Canada: Non-stationarity and teleconnection to climate patterns. *Science of the Total Environment*, *746*, 141330. https://doi.org/10.1016/j.scitotenv.2020.141330

Wu, Y., Long, D., Lall, U., Scanlon, B. R., Tian, F., Fu, X., et al. (2022). Reconstructed eight-century streamflow in the Tibetan Plateau reveals contrasting regional variability and strong nonstationarity. *Nature Communications*, *13*(1), 6416. https://doi.org/10.1038/s41467-022-34221-9

Wu, Z., & Huang, N. E. (2009). Ensemble empirical mode decomposition: A noise-assisted data analysis method. *Advances in Adaptive Data Analysis*, *1*(1), 1–41. https://doi.org/10.1142/S1793536909000047

Xu, Z., Han, Y., Tam, C. Y., Yang, Z. L., & Fu, C. (2021). Bias-corrected CMIP6 global dataset for dynamical downscaling of the historical and future climate (1979–2100). *Scientific Data*, *8*(1), 293. https://doi.org/10.1038/s41597-021-01079-3

Yan, H., Zhao, N., Zhou, P., Liu, C., Fei, H., Li, M., et al. (2021). The first detection of the Madden-Julian Oscillation signal in daily to hourly resolution proxy records derived from a natural archive of Giant Clam Shell (Tridacna spp.). *Earth and Planetary Science Letters*, *555*, 116703. https://doi.org/10.1016/j.epsl.2020.116703

Yan, J. (2007). Enjoy the Joy of Copulas: With a Package copula. *Journal of Statistical Software*, *21*(4), 1–21. https://doi.org/10.18637/jss.v021.i04

Yao, T., Bolch, T., Chen, D., Gao, J., Immerzeel, W., Piao, S., et al. (2022). The imbalance of the Asian water tower. *Nature Reviews Earth & Environment*, *3*(10), 618–632. https://doi.org/10.1038/s43017-022-00299-4

Yi, S., Saemian, P., Sneeuw, N., & Tourian, M. J. (2023). Estimating runoff from pan-Arctic drainage basins for 2002–2019 using an improved runoff-storage relationship. *Remote Sensing of Environment*, *298*, 113816. https://doi.org/10.1016/j.rse.2023.113816

Yue, W., & Chen, F. (2025). Runoff reconstructions and future projections indicate highly variable water supply from Pacific Rim water towers (Version 1) [Dataset]. *Mendeley Data*. https://doi.org/10.17632/wh5g9hwv5g.1

Yue, W., Chen, F., Davi, N. K., Zhang, H., Chen, Y., Zhao, X., & Gao, Z. (2024). Little Ice Age cooling in the Western Hengduan Mountains, China: A 600-year warm-season temperature reconstruction from tree rings. *Climate Dynamics*, *62*(1), 773–790. https://doi.org/10.1007/s00382-023-06932-2

Yue, W., Chen, F., Solomina, O., Esper, J., Davi, N. K., Büntgen, U., et al. (2025). Drought facilitated the westward expansion of the Mongol Empire in the 1230s. *Fundamental Research*. https://doi.org/10.1016/j.fmre.2025.08.010

Yue, W., Chen, F., Torbenson, M. C. A., Zhao, X., Zheng, Y., Xu, Y., et al. (2024). Late Ming Dynasty weak monsoon induced a harmonized megadrought across north-to-south China. *Communications Earth & Environment*, *5*(1), 439. https://doi.org/10.1038/s43247-024-01602-5

Yue, W., Seftigen, K., Chen, F., Wilson, R., Zhang, H., Miao, Y., et al. (2023). Picea schrenkiana tree ring blue intensity reveal recent glacier mass loss in High Mountain Asia is unprecedented within the last four centuries. *Global and Planetary Change*, *228*, 104210. https://doi.org/10.1016/j.gloplacha.2023.104210

Zhang, Q., Miao, C., Gou, J., Wu, J., Jiao, W., Song, Y., & Xu, D. (2022). Spatiotemporal characteristics of meteorological to hydrological drought propagation under natural conditions in China. *Weather and Climate Extremes*, *38*, 100505. https://doi.org/10.1016/j.wace.2022.100505

Zhao, X., Fang, K., Chen, F., Martín, H., & Roig, F. A. (2023). Reconstructed Jing River streamflow from western China: A 399-year perspective for hydrological changes in the Loess Plateau. *Journal of Hydrology*, *621*, 129573. https://doi.org/10.1016/j.jhydrol.2023.129573

Zhao, Y., Xu, C., Liu, Y., An, W., & Guo, Z. (2023). Irrawaddy River experienced more frequent hydrological drought events with global warming: Evidence from a 400-year tree ring oxygen isotope record. *Catena*, *232*, 107455. https://doi.org/10.1016/j.catena.2023.107455

Zhu, Q., & Cai, Y. (2023). Integrating ecological risk, ecosystem health, and ecosystem services for assessing regional ecological security and its driving factors: Insights from a large river basin in China. *Ecological Indicators*, *155*, 110954. https://doi.org/10.1016/j.ecolind.2023.110954

Ziaco, E., Miley, N., & Biondi, F. (2020). Reconstruction of seasonal and water-year precipitation anomalies from tree-ring records of the southwestern United States. *Palaeogeography, Palaeoclimatology, Palaeoecology*, *547*, 109689. https://doi.org/10.1016/j.palaeo.2020.109689

Zou, H., & Hastie, T. (2005). Regularization and variable selection via the elastic net. *Journal of the Royal Statistical Society Series B: Statistical Methodology*, *67*(2), 301–320. https://doi.org/10.1111/j.1467-9868.2005.00503.x